

Tabulated chemistry approaches for laminar flames: Evaluation of flame-prolongation of ILDM and flamelet methods

Pradeep K. Jha* and Clinton P.T. Groth

University of Toronto Institute for Aerospace Studies, 4925 Dufferin Street, Toronto, Ontario, Canada M3H 5T6

(Received 25 November 2010; final version received 6 July 2011)

The present study considers the performance of tabulation methods for numerical simulation of complex chemical kinetics in laminar combusting flows and compares their predictions to results obtained by direct calculation. Two tabulation methods are considered: the Flame Prolongation of Intrinsic low-dimensional manifold (FPI) method and Steady Laminar Flamelet Model (SLFM). The FPI method is of current interest as it is a potentially unifying approach capable of dealing with both premixed and non-premixed flames for gaseous fuels. SLFM tabulation methods are popular for non-premixed flames and form a good basis for comparing the performance of the FPI approach. The performance of each method is also evaluated by comparing the results to the direct simulation of the laminar flames using two chemical kinetic schemes: simplified chemistry involving five species and one reaction and detailed chemistry involving 53 species and 325 reaction steps. As part of the evaluation process, the computational cost of each method is also assessed. The laminar flames considered in this study include: freely propagating laminar premixed flames, a two-dimensional axisymmetric methane–air opposed-jet diffusion flame, and a two-dimensional axisymmetric methane–air co-flow diffusion flame. Both tabulation methods are implemented in a parallel adaptive mesh refinement (AMR) framework for solving the complete set of governing partial differential equations. These equations are solved using a fully-coupled finite-volume formulation on body-fitted multi-block quadrilateral mesh. Significant improvements in terms of reduced computational requirements, as measured by both storage and processing time, are demonstrated for the tabulated methods.

Keywords: numerical combustion modelling; laminar flames; chemical kinetics; tabulated chemistry; adaptive mesh refinement (AMR)

1. Introduction

A major challenge in the simulation of combustion processes is the modelling and evaluation of reaction rates for accurately representing chemical kinetics. Direct numerical simulations (DNS) of large complex reaction mechanisms place heavy demands on computational resources in terms of processor time, memory and storage requirements. This has prompted researchers to consider computationally efficient approaches for modelling the chemical kinetics without significantly compromising the quality of results. Although not fully inclusive, the computationally efficient techniques for the treatment of complex chemistry in combustion processes can be broadly categorized into two groups [1]:

*Corresponding author. Email: jhapk@utias.utoronto.ca

(i) chemical reduction techniques; and (ii) flamelet approaches. The *in Situ* Adaptive Tabulation (ISAT) approach proposed by Pope [2], based on the generation of look-up tables for chemical kinetics during direct simulations, falls somewhat outside this classification, but the classification is still useful nonetheless.

Chemical Reduction Techniques (CRT) are based on the observation that chemical processes are mainly determined by a small number of slow reactions. These methods assume that species involved in fast reaction processes are in a near quasi-equilibrium steady state. Computational savings are garnered by tracking only the finite-rate reactions and species involved in slow processes. CRT differ from each other mainly in how the fast and slow processes are determined and handled. The Systematic Reduction Method (SRM), as discussed in the review by Peters [3], invokes a steady-state assumption for species involved in fast chemical processes. This however involves a detailed study of all reaction steps and time-scales, which can become quite involved for fuels with complex molecular structure [4]. The Computational Singular Perturbation (CSP) method proposed by Lam and Goussis [5] examines the Jacobian of the local chemical source terms to identify slow processes. CSP is quite accurate; however, slow processes are calculated dynamically and the number of steady-state variables varies continuously during the simulation, which can make the method computationally expensive. The Intrinsic Low Dimensional Manifold (ILDM) approach, proposed by Mass and Pope [6], is based on the analysis of the eigenstructure of the Jacobian of the local chemical source terms to identify slow chemical processes. Based on this eigensystem analysis, a small subset of variables is identified which evolves slowly during combustion. These variables are then used to generate pre-computed look-up tables to be used during simulations for evaluating chemical kinetics. The ILDM method has been shown to fail in regions of flow where diffusion processes are as important as chemical processes and it generally does not yield good results in low temperature regions of flames as fast time-scales have been neglected. The Trajectory Generated Low Dimensional Manifold (TGLDM) is based on the same principles as the ILDM method, however, instead of the chemical reacting system, the TGLDM system computes a manifold using trajectories [7]. The trajectory is the path the system takes through composition space from the initial point to the chemical equilibrium composition. TGLDM methods have the advantage over ILDM methods that they guarantee convergence and that the reaction vector is always tangent to the trajectory. A disadvantage is that it is not yet clear how one can incorporate the effects of diffusion on the manifold with TGLDM methods, as has been done with ILDM methods [8].

Flamelet approaches assume that the local chemical structure of a flame is independent of the physical complexity of the surrounding flow. Pre-generated solutions of chemical composition for simple flames are used to predict local chemical composition in more complex situations using solution mapping procedures and functions. Flamelet methods have become popular for the treatment of diffusion flames over the last 10–15 years. Several past attempts have been made to study the chemical properties of a diffusion flame as a function of one conserved scalar (Bilger [9], Libby and Williams [10]). In the Steady Laminar Flamelet Model (SLFM) of Peters [11], pre-computed detailed chemistry solutions of one-dimensional counter-flow flames are used for the simulation of more general diffusion flames. For this, all flame properties at any point in the flow are expressed in terms of mixture fraction and another scalar characterizing the dissipation of the mixture fraction [11]. Subsequent follow-on studies have considered the application of this formulation [12–14]. Smooke *et al.* [15] and Nishioka *et al.* [16] have compared multi-dimensional laminar diffusion flame simulation results to one-dimensional counter-flow flames and reported that there is good agreement between the structure of the two flames. Smooke *et al.* [15]

observed that the flamelet model yields poor predictions for some species concentrations in fuel-rich regions. In a recent study of the flamelet model for laminar flames, Liu *et al.* [14] compared directly-calculated solutions with those of the flamelet approach for a co-flow diffusion flame and noted that numerical results depend quantitatively on the definition of dissipation rate and mixture fraction.

Flame-Prolongation of ILDM (FPI) and Flame-Generated Manifold (FGM) are two tabulated approaches developed independently by Gicquel *et al.* [17] and Oijen *et al.* [4], respectively. The two methods are conceptually similar and can be viewed as hybrids of the CRT and flamelet methods discussed above. They both use pre-tabulated solutions of flames that have simplified flow geometry, which are subsequently used for the simulation of more complex flames. A controlling parameter, called the progress of reaction variable, is introduced to define the mapping between the tabulated solutions and local solutions within a combustion simulation. When detailed solutions of one-dimensional laminar premixed flames are used as the basis for the tabulation in the FPI approach, both FPI and FGM are essentially identical. The primary differences between the methods are then technical and relate simply to how the tabulated data is constructed and accessed. The FGM approach is based on tabulating data as a function of enthalpy and progress of reaction variable, while FPI stores data as a function of the mixture fraction and progress of reaction variable.

The FPI and FGM schemes are currently of great interest as they are potentially unifying approaches which can be applied to the full range of flames, i.e., premixed, partially-premixed, and non-premixed flames. For laminar premixed flames, Gicquel *et al.* [17] and Oijen *et al.* [4] indicated that their respective approaches are much faster than directly performing calculations with detailed chemistry. The FPI method was extended to diffusion flames by Vervisch *et al.* [18] and for non-adiabatic flames by Fiorina *et al.* [19]. Fiorina *et al.* [20] subsequently also assessed the performance of the FPI method for one-dimensional counter-flow flames. More recently, Galpin *et al.* [21] have examined different ways in which the FPI approach can be coupled to reactive flow solution methods. Additionally, both FPI and FGM have been successfully applied in computations of complex turbulent combusting flows [21–25].

Although the FPI and flamelet methods have already been developed and applied to turbulent combusting flows as indicated above, it can still be very instructive to consider their application and performance to laminar flames. Such studies provide valuable insight into understanding and interpreting the capabilities of these approximate techniques when applied to turbulent flames, which is of course the ultimate objective. Moreover, as the FPI has been shown to have considerable potential when applied to various combustion regimes, i.e., to autoignition [24], lifted flames [25], and unsteady flames, a performance review of the method for laminar flames would seem particularly important and timely. With this viewpoint, the performance of FPI and the SLFM schemes are both compared herein for selected laminar flames. The accuracy and computational costs of the FPI and SLFM methods are assessed and discussed.

2. Tabulation methods for chemical kinetics

2.1. Steady laminar flamelet model

The SLFM approach expresses all of the local thermochemical properties of a diffusion flame as a function of a single conserved scalar. This approach is based on the observation that the reaction zones in diffusion flames are limited to a thin region where reactants mix with each other in a stoichiometric ratio. Hence, the local instantaneous reaction zone

structure is assumed to be the same as that of a quasi-steady one-dimensional laminar flame [11].

The mixing at any point in the flow is defined by a scalar field called the mixture fraction, f , defined as the ratio of the mass of the material having its origin in the fuel stream to the total mass of the mixture [26]. The values of the mixture fraction vary from zero in the oxidizer feed to one in the fuel feed. Peters [11] has previously derived the flamelet equation of chemical species, k , having a mass fraction, Y_k , which for unity Lewis numbers can be written as

$$\rho \frac{\partial Y_k}{\partial t} = \rho \frac{\chi}{2} \frac{\partial^2 Y_k}{\partial f^2} + \dot{\omega}_k, \quad (k = 1, \dots, N) \quad (1)$$

where

$$\chi = 2D_f \frac{\partial f}{\partial x_i} \frac{\partial f}{\partial x_i} \quad (2)$$

and where $\dot{\omega}_k$ is the mass reaction rate of species k produced by the chemical reactions, ρ is the mixture density, and χ is the scalar dissipation rate. Under the assumptions of unity Lewis number and further neglecting unsteady pressure changes and radiation heat transfer, it can be shown that the transport equation for the mixture fraction is equivalent to that for the mixture enthalpy (a conserved scalar, see Section 3.2) and the diffusion coefficient of the mixture fraction, D_f , is equal to the thermal diffusivity of the mixture and given by $D_f = \lambda / \rho C_p$ where λ is the mixture thermal conductivity and C_p is the gas specific heat at constant pressure [26].

The steady-state form of Equation (1) can be solved numerically using well developed methodologies and software. Here, Cantera [27], an open-source software package for chemically-reacting flows, is used to obtain steady-state solutions for counter-flow diffusion flames having different strain rates and hence different ranges of the scalar dissipation rates. Note that Cantera does not solve Equation (1) directly. Instead self-similar solutions are computed to the full low-Mach-number-limit Navier–Stokes equations for a reactive ideal gas mixture in an axisymmetric flow domain with an infinite radial extent. The approach allows for arbitrary chemistry and arbitrary variation of the transport properties and is not limited to the assumption of unity Lewis number for species mass transport. Note however, the assumption of unity Lewis number is somewhat implicit in the derivation of the transport equation for the mixture fraction and the assumption that the diffusion coefficient for the mixture fraction is equal to the thermal diffusivity. For situations where this is not true, there is some inconsistency in the flamelet formulation as defined herein, although appropriate modifications are possible as outlined by Pitsch and Peters [28].

Solutions for a series of strain rates, ranging from small values (near equilibrium) to very large values (approaching the quenching limit) are calculated using the Cantera software package. In the present work, the characteristic strain rate value for the counter-flow flame is defined as the velocity gradient at the stagnation point. While Equation (1) clearly indicates that the value of χ varies throughout the laminar flame solution, a single characteristic value of the scalar dissipation rate is chosen to represent the solution for each characteristic strain rate. Since most of the chemical activity occurs in the vicinity of the stoichiometric point of the flame, it is usually adequate to take the value of the scalar dissipation rate where mixture fraction is equal to the stoichiometric value, χ_{st} , as the representative characteristic value [11, 14]. Some authors also use the value of χ at the maximum temperature as the

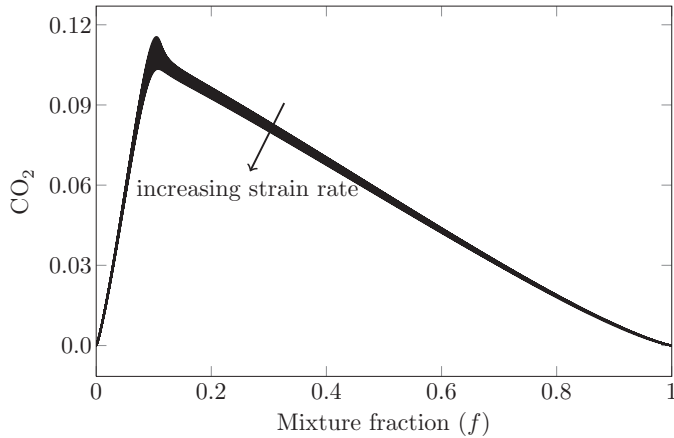


Figure 1. Variation of concentration of CO₂ in the mixture fraction space for different values of the strain rate.

characteristic rate [29]. For the methane–air flames being studied in this paper, these values are virtually identical and thus the stoichiometric dissipation rate, χ_{st} , is used here.

The counter-flow diffusion flame solutions are stored in a flamelet library such that any thermochemical quantity, φ , can be retrieved and expressed as $\varphi^{FL} = \varphi(f, \chi_{st})$. For general combusting flows, the balance equation for the mixture fraction, f , is then solved instead of the full set of species continuity equations, and the local scalar dissipation rate, χ , is calculated at each point using Equation (2). Local values of f and χ are used to obtain the local chemical composition from the flamelet library using a bi-linear interpolation procedure. Peters [11] mentions that NO_x and soot particles are particularly sensitive to χ , but as the present work does not consider the formation of either of these pollutants, the variation in species concentration as a function of scalar dissipation rate should not be a significant factor. Figure 1 shows the change in concentration of CO₂ for different strain rate values. Similar behaviour is also observed for other thermochemical quantities. The effect of the number of tabulated strain rates is discussed further in Section 4.3.

For the methane–air flames of interest here, two SLFM tabulation approaches are considered:

- **Approach 1:** The local values of f and χ are used to obtain mass fractions from the flamelet library. A consistent solution for the mixture temperature, T , is obtained by solving the energy equation.
- **Approach 2:** Both mass fractions and temperature, T , are read from the flamelet library as a function of local value of f and χ . The energy equation is not solved.

The results and performance of both of these two approaches are discussed in Section 4.

2.2. Flame Prolongation of ILDM (FPI)

2.2.1. Tabulation of detailed chemistry solutions

In the FPI approach, every thermochemical quantity, φ , is expressed as a function of two independent variables: the mixture fraction, f , and progress of reaction variable, Y_c . For a pure-mixing/non-reacting situation the local value of any quantity, φ , can be expressed as

a linear function of the mixture fraction, f , using the relation

$$\varphi = f\varphi_{F,o} + (1 - f)\varphi_{O,o} \quad (3)$$

where $\varphi_{F,o}$ is the value of φ in the fuel stream and $\varphi_{O,o}$ is the value of φ in the oxidizer stream. For a given equivalence ratio, ϕ , all flame properties of a one-dimensional laminar premixed flame can be expressed as $\varphi = \varphi(\phi, x)$ where x is the spatial coordinate in the direction normal to the flame front. Using Equation (3) and the equivalence ratio, f can then be expressed uniquely as a function of ϕ as

$$f(\phi) = \frac{\phi}{\left(\phi + s \frac{Y_{F,o}}{Y_{O,o}}\right)} \quad (4)$$

where s is the stoichiometric oxidizer-fuel mass ratio. For simple hydrocarbons, Y_c can be defined as a linear combination of the species mass fractions, Y_i , and written as

$$Y_c(\phi, x) = \sum_{j=1}^N \alpha_j Y_j(\phi, x) \quad (5)$$

such that there is a one-to-one correspondence between x and Y_c , for a given equivalence ratio. Using this expression, the spatial coordinate, x , can be eliminated and the final FPI tabulation is then carried out as follows:

$$\varphi^{\text{FPI}} = \varphi(\phi, x) = \varphi(f(\phi), Y_c(x)). \quad (6)$$

The choice of Y_c varies from fuel to fuel. For methane-air flames, Fiorina *et al.* [19] propose that a linear combination of the mass fraction of CO and CO₂ is a good choice for Y_c . For practical considerations [18], a normalized value of Y_c , called the progress variable, c , is introduced. The progress variable, as illustrated in Figure 2(a), is defined as

$$c = \frac{Y_c(\phi, x)}{Y_c^{\text{EQ}}(\phi, x)} \quad (7)$$

where Y_c^{EQ} is the value of Y_c in the burnt state of the laminar-premixed flame. The final FPI look-up table for laminar flames is then of the form

$$\varphi^{\text{FPI}} = \varphi(f, c). \quad (8)$$

As with the SLFM, the Cantera package [27], based on the GRI-Mech 3.0 mechanism, is again used to obtain detailed chemistry solutions for one-dimensional premixed flames for different equivalence ratios within the flammability limits of premixed flames.

For premixed flames, a number of studies have reported on the validity of the preceding approach [19, 20, 30]. However, for diffusion flames, the mixture fraction values can lie outside the flammability limits of premixed flames and take on values anywhere from zero to one. To calculate the mass fractions for points lying outside the range of valid premixed flame solutions, a linear interpolation is performed between the rich/lean flammability limit solution and the pure-mixing solution given by Equation (3). This approach, illustrated in Figure 2(b), differs somewhat from methods proposed previously [18, 31]. The reaction

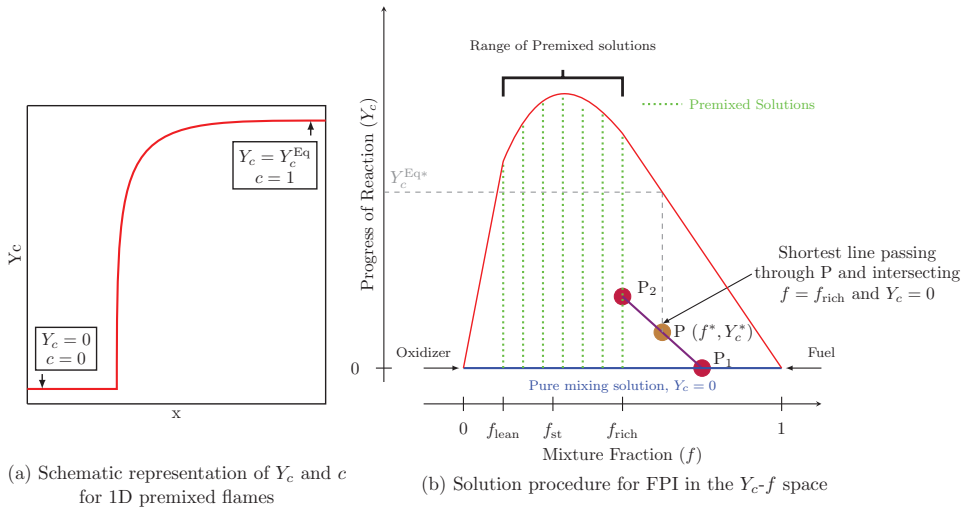


Figure 2. Schematic diagrams illustrating the algorithm used for interpolation of FPI tabulated flamelet data.

rates are also set to zero outside the premixed flame flammability limits. It should be noted that diffusion flamelets could potentially be used to create the tabulated chemistry manifold as discussed by Delhaye *et al.* [1], but this has not been considered here. The focus of the present study is an evaluation of the FPI approach based on premixed laminar flamelets.

2.2.2. Coupling tabulated data with reactive flow solution algorithm

The FPI table size can be an important concern and can tax available computer memory when performing practical calculations, especially when dealing with non-premixed turbulent flames. Galpin *et al.* [32] have shown that of the 53 GRI-Mech 3.0 mechanism species, only seven species: CH₄, O₂, CO₂, CO, H₂O, H₂ and N₂, are needed to account for more than 99.5% of the total mass and energy of the mixture. Therefore, using the information for only these seven species affords virtually a full description of the flame properties. However, in order to properly account for the elemental mass of the remaining species, additional species must also be tabulated. Careful studies have shown that H, OH and C₂H₂ are a good choice for these additional species in the case of methane–air flames [32]. Hence, the final look-up table in the current study stores data for a total of 10 species (seven major and three minor species).

Three approaches are considered here for coupling the FPI tabulated data to the reactive flow solution algorithm used here:

- Approach 1 – Tabulated mass fractions:** The look-up table stores the mass fractions of the reduced set of species. The mass fractions of the major species are used directly from the pre-computed solutions whereas the mass fractions of minor or additional species, such as C₂H₂ and H₂, are calculated by ensuring atomic mass conservation [21]. For example, when the detailed chemistry solution of all 53 species is known, the conservation of atomic mass of carbon atoms provides the following expression for

calculating $Y_{C_2H_2}$ in the reduced set of species:

$$Y_{C_2H_2} = \frac{MW_{C_2H_2}}{n_{C_2H_2}} \left(\sum_{j=1}^N Y_j \frac{n_{C_j} AW_C}{MW_j} - \sum_{\substack{j=1 \\ j \neq C_2H_2}}^M Y_j \frac{n_{C_j} AW_C}{MW_j} \right) \quad (9)$$

where N is the total number of species, M is the number of species in the reduced set, n_{C_j} is the number of carbon atom in species j , AW_j is the atomic weight of species j , and MW_j is the molecular weight of species j .

Individual species transport equations are not solved. Instead, local values of f and Y_c are used to obtain the species concentrations from the table using bi-linear interpolation.

- **Approach 2 – Tabulated reaction rates:** The look-up table stores the reaction rates of the reduced set of species. The reaction rates of the major species are used directly from the pre-computed solutions but the reaction rates of the additional minor species are evaluated by using atomic mass conservation [21]. For example, conservation of atomic mass of carbon atoms gives the following expression for $\dot{\omega}_{C_2H_2}$:

$$\dot{\omega}_{C_2H_2} = -\frac{MW_{C_2H_2}}{n_{C_2H_2}} \sum_{\substack{j=1 \\ n_{C_j} \neq 0 \\ j \neq C_2H_2}}^M \frac{\dot{\omega}_j}{MW_j}. \quad (10)$$

The transport equations for the mass fractions of each species in the reduced set, both major and minor species, are solved. The tabulated reaction rates stored as a function of local values of f and Y_c are used in evaluating the chemical source terms appearing in the species transport equations.

- **Approach 3 – Tabulated mass fractions & estimated reaction rates:** Highly diffusive species can have large gradient values. Resolving these high values using tabulated species mass fraction needs highly refined tables. A bridge between the above two approaches is to use a mass fraction look-up table, like Approach 1, and reconstruct the species reaction rates using this mass fraction data. Domingo *et al.* [23] have shown that in a laminar premixed flame, the source terms are related by

$$\dot{\omega}_i = \dot{\omega}_{Y_c} \left[\frac{\partial Y_i}{\partial Y_c} - \frac{1}{Da} \left(\frac{\partial^2 Y_i}{\partial Y_c^2} \right) \right] \quad (11)$$

where Da is the Damköhler number. For fast chemistry and large values of Da , the second term can be neglected to yield the simplified expression

$$\dot{\omega}_i \approx \dot{\omega}_{Y_c} \frac{\partial Y_i}{\partial Y_c}. \quad (12)$$

The species mass balance equations are then solved directly using the above expression. This approach avoids the need for a large number of tabulated values as in Approach 2 to account for the wide ranges in the magnitude of the reaction rates for the more diffusive species.

In all of the above approaches, the conservation equations for mass, momentum, and energy are solved along with transport equations for the mixture fraction and progress of reaction

Table 1. Different ways of coupling the FPI look-up table to the flow solver. In all methods, $\dot{\omega}_{Y_c}$ for Y_c transport equation is obtained from the table.

Approach	Tabulated data	Species PDEs solved	Solution methodology
1	$Y_i, \dot{\omega}_{Y_c}$	No	Get Y_i from table using $Y_i = Y_i(f, Y_c)$. Use Y_i directly in the solver.
2	$\dot{\omega}_i, \dot{\omega}_{Y_c}$	Yes	Get $\dot{\omega}_i$ from table using $\dot{\omega}_i = \dot{\omega}_i(f, Y_c)$. Use $\dot{\omega}_i$ in species PDEs for reaction rate source term.
3	$Y_i, \dot{\omega}_{Y_c}$	Yes	Get Y_i from table. Reconstruct $\dot{\omega}_i$ using $\dot{\omega}_i \approx \dot{\omega}_{Y_c} \frac{\partial Y_i}{\partial Y_c}$. Use these $\dot{\omega}$ values in species PDEs.

variable. Table 1 summarizes these approaches. Note that for FPI tabulation, a formulation similar to the SLFM-Approach 2, in which the temperature is directly obtained from the tables and the energy equation is not solved, was not considered here.

The FPI, and for that matter, the SLFM tabulation methods are both coupled to a density-based solution algorithm of the compressible form of the Navier–Stokes equations for a reactive mixture (the solution method and governing equation are summarized in the next section of the paper to follow). However, as all of the laminar flames considered in the present study are both steady and essentially isobaric, and radiation losses are not significant, the coupling of the tabulation methods with the solution algorithm was rather straightforward. The tabulations were performed for a single pressure (atmospheric pressure) and any small variations in pressure from the reference condition were ignored when using and accessing the tables. Nevertheless, for more general combustion processes involving non-adiabatic flames with acoustical phenomena and/or significant pressure variations, coupling of the tabulation methods to a compressible-flow solution method would be more involved and a multi-pressure tabulation procedure may be required. Issues of coupling of the FPI and SLFM methods to a solution algorithm for the governing flow equations is not the primary focus here. Galpin *et al.* [32] and the recent paper by Vicquelin *et al.* [33] discuss coupling of tabulated chemistry methods with various solution methods for the flow equations.

3. Governing equations and numerical scheme

3.1. Navier–Stokes equations for a reactive mixture

Neglecting soot formation and radiation transport, laminar flames can be fully described by the Navier–Stokes equations for a compressible, thermally-perfect, reactive mixture governing the conservation of mass, momentum, and energy for the mixture and the transport of mass for each of the individual species. The balance equations in tensor notation for a N -species reactive mixture are given by [34, 35]

$$\frac{\partial \rho}{\partial t} + \frac{\partial}{\partial x_i} (\rho u_i) = 0 \quad (13)$$

$$\frac{\partial}{\partial t} (\rho u_i) + \frac{\partial}{\partial x_j} (\rho u_j u_i) = -\frac{\partial p}{\partial x_i} + \frac{\partial \tau_{ji}}{\partial x_j} + G_i \quad (14)$$

$$\frac{\partial}{\partial t} (\rho Y_k) + \frac{\partial}{\partial x_j} (\rho u_j Y_k) = -\frac{\partial \mathcal{J}_j^k}{\partial x_j} + \dot{\omega}_k \quad (15)$$

$$\frac{\partial}{\partial t} (\rho e) + \frac{\partial}{\partial x_j} \left[\rho u_j \left(e + \frac{p}{\rho} \right) \right] = \frac{\partial}{\partial x_j} (u_i \tau_{ij}) - \frac{\partial q_j}{\partial x_j} + u_i G_i. \quad (16)$$

The molecular heat flux vector is given by

$$q_j = -\lambda \frac{\partial T}{\partial x_j} + \sum_{k=1}^N Y_k h_k u_j. \quad (17)$$

The mixture pressure is given by the ideal gas law, $p = \sum_{k=1}^N \rho Y_k R_k T$. The fluid is assumed to be Newtonian and so the viscous stress tensor has the form

$$\tau_{ij} = \mu \left(\frac{\partial u_i}{\partial x_j} + \frac{\partial u_j}{\partial x_i} \right) - \frac{2}{3} \delta_{ij} \frac{\partial u_k}{\partial x_k}. \quad (18)$$

Species molecular diffusivity is determined using Fick's law and given by

$$\mathcal{J}_j^k = -\frac{\mu}{Sc_k} \frac{\partial Y_k}{\partial x_j} \quad (19)$$

where

$$Sc_k = \frac{\mu}{\rho D_k}. \quad (20)$$

In the expressions above, ρ is the mixture density, \vec{u} is the velocity vector, p is the pressure, τ is the viscous force tensor, \vec{g} is the body force vector, Y_k is the mass fraction of species k , $\dot{\omega}_k$ is again the mass reaction rate of species k produced by the chemical reactions, $\vec{\mathcal{J}}^k$ is the molecular diffusive flux of the species k , e is the specific total energy ($u_i u_i / 2 + h - p / \rho$), h is the internal energy $\sum_{k=1}^N Y_k h_k$, h_k is the absolute internal enthalpy for species k , \vec{q} is the molecular heat flux vector, R_k is the gas constant of species k , T is the mixture temperature, λ is again the mixture thermal conductivity, μ is the molecular viscosity depending on fluid properties, δ_{ij} is the Kronecker delta function, Sc_k is the Schmidt number of species k , and D_k is the molecular diffusivity of the species k relative to mixture.

3.2. Additional balance equations

Both the FPI and the SLFM approach use the mixture fraction variable, f , to obtain the chemical composition at any point in the flow from the look-up table. The FPI tabulation is also dependent on another parameter called the progress of reaction, Y_c . The balance equations for these two scalar variables are given by

$$\frac{\partial}{\partial t} (\rho f) + \frac{\partial}{\partial x_i} (\rho u_i f) = \frac{\partial}{\partial x_i} \left(\rho D_f \frac{\partial f}{\partial x_i} \right) \quad (21)$$

$$\frac{\partial}{\partial t} (\rho Y_c) + \frac{\partial}{\partial x_i} (\rho u_i Y_c) = \frac{\partial}{\partial x_i} \left(\rho D_{Y_c} \frac{\partial Y_c}{\partial x_i} \right) + \rho \dot{\omega}_{Y_c} \quad (22)$$

where $D_{Y_c} = \mu / \rho Sc_{Y_c}$ is the diffusion coefficient of Y_c , $\dot{\omega}_{Y_c}$ is the reaction rate of Y_c (sum of the reaction rates of all the species defining Y_c), and Sc_{Y_c} is the Schmidt number for the progress of reaction variable. In the FPI model, the latter is taken to have a constant

value of unity herein. Although other choices and even a variable Schmidt number are possible, these are not considered here as the value of the Schmidt number does not appear to significantly affect the predictions for the flames of interest here.

The source term, $\dot{\omega}_{Y_c}$, appears in Equation (22). In FPI tabulation, this value is also stored in the look-up table as a function of Y_c and f . The value is obtained from the table along with the species mass fraction and/or reaction rates, as a function of local values of Y_c and f .

3.3. Conservation form of equations

For two-dimensional axisymmetric flows, the preceding equations governing a reactive compressible mixture can be re-expressed using vector notation as

$$\frac{\partial \mathbf{U}}{\partial t} + \frac{\partial}{\partial r} (\mathbf{F} - \mathbf{F}_v) + \frac{\partial}{\partial z} (\mathbf{G} - \mathbf{G}_v) = \frac{1}{r} (\mathbf{S}_\phi + \mathbf{S}_{\phi v}) + \mathbf{S} \quad (23)$$

where \mathbf{U} is the vector of conserved variables given by

$$\mathbf{U} = [\rho, \rho v_r, \rho v_z, \rho e, \rho Y_1, \dots, \rho Y_n, \rho f, \rho Y_c]^T \quad (24)$$

and r and z are the radial and axial coordinates of the axisymmetric frame. The inviscid and viscous radial flux vectors, \mathbf{F} and \mathbf{F}_v , are

$$\mathbf{F} = [\rho v_r, \rho v_r^2 + p, \rho v_r v_z, (\rho e + p)v_r, \rho v_r Y_1, \dots, \rho v_r Y_n, \rho v_r f, \rho v_r Y_c]^T \quad (25)$$

$$\mathbf{F}_v = \left[0, \tau_{rr}, \tau_{rz}, v_r \tau_{rr} + v_z \tau_{rz} - q_r, -\mathcal{J}_r^1, \dots, -\mathcal{J}_r^n, \rho D_f \frac{\partial f}{\partial r}, \rho D_{Y_c} \frac{\partial Y_c}{\partial r} \right] \quad (26)$$

and the inviscid and viscous axial flux vectors, \mathbf{G} and \mathbf{G}_v , are

$$\mathbf{G} = [\rho v_z, \rho v_r v_z, \rho v_z^2 + p, (\rho e + p)v_z, \rho v_z Y_1, \dots, \rho v_z Y_n, \rho v_z f, \rho v_z Y_c]^T \quad (27)$$

$$\mathbf{G}_v = \left[0, \tau_{zr}, \tau_{zz}, v_r \tau_{zr} + v_z \tau_{zz} - q_z, -\mathcal{J}_z^1, \dots, -\mathcal{J}_z^n, \rho D_f \frac{\partial f}{\partial z}, \rho D_{Y_c} \frac{\partial Y_c}{\partial z} \right]^T \quad (28)$$

The source terms, \mathbf{S}_ϕ and $\mathbf{S}_{\phi v}$, are the inviscid and viscous source vectors associated with the axisymmetric geometry, respectively. The source vector, \mathbf{S} , contains terms related to the finite rate chemistry and body force due to gravity. These three source vectors have the respective forms:

$$\mathbf{S}_\phi = [-\rho v_r, -\rho v_r^2, -\rho v_r v_z, -\rho v_r (\rho e + p), -\rho v_r Y_1, \dots, -\rho v_r Y_n, -\rho v_r f, -\rho v_r Y_c]^T \quad (29)$$

$$\mathbf{S}_{\phi v} = \left[0, \tau_{rr} - \tau_{\theta\theta}, \tau_{rz}, v_r \tau_{rr} + v_z \tau_{rz} - q_r, -\mathcal{J}_r^1, \dots, -\mathcal{J}_r^n, \rho D_f \frac{\partial f}{\partial r}, \rho D_{Y_c} \frac{\partial Y_c}{\partial r} \right]^T \quad (30)$$

$$\mathbf{S} = [0, 0, \rho g_z, \rho v_z g_z, \rho \dot{\omega}_1, \dots, \rho \dot{\omega}_n, 0, \rho \dot{\omega}_{Y_c}]^T \quad (31)$$

3.4. Parallel block-based AMR finite-volume solution method

For the direct-calculation of the laminar flames considered here, the preceding system of non-linear conservation laws governing a compressible, thermally-perfect, reactive gaseous mixture are solved numerically using a parallel, fully-coupled, finite-volume scheme with block-based AMR on a body-fitted, multi-block, quadrilateral computational mesh previously developed by Groth and co-workers [36–39]. The scheme makes use of piecewise limited linear reconstruction and Riemann-solver-based flux functions to determine the inviscid flux. A second-order diamond-path discretization method is used for the viscous fluxes. The solution of the fully-coupled non-linear ODEs is obtained via a method of lines approach. This fully-coupled density-based approach for the compressible-form of the Navier–Stokes equations uses low-Mach-number preconditioning to deal with the low-speed flows associated with the laminar flames. A more complete description of the solution methodology used here is given in the papers by Northrup and Groth [36], Charest *et al.* [38], and Gao *et al.* [37, 39].

In order to allow a direct and meaningful comparison of the direct-calculated laminar flame results to those of the tabulated chemistry results, all thermodynamic and transport properties for the reactive mixture, along with chemical kinetic rates, are again evaluated using Cantera [27], the open-source software package for chemically-reactive flows used in the generation of the SLFM and FPI tables. The diffusive velocity for each species is evaluated in Cantera using mixture-averaged diffusion coefficients [40]. Wilke’s formula is used for the mixture-averaged viscosity [41] and a combination-averaging formula is utilized for the mixture-averaged thermal conductivity [42]. For the methane–air flames considered in this study, results were obtained for two reaction mechanisms: a simplified one-step, five-species, chemical kinetic scheme proposed by Westbrook and Dryer [43] and a detailed Gri-Mech 3.0 mechanism involving 53 species and 325 reactions [44]. The one-step reduced mechanism is considered herein merely as a baseline for comparison of computational costs and not for any assessment of the accuracy of the tabulated chemistry approaches.

The parallel, block-based, AMR scheme described above was modified to allow for the use of the SLFM and FPI tabulated-chemistry methods of primary interest here and to perform the table generation. Coupling of these two tabulation methods to the solution algorithm is described in Sections 2.1 and 2.2.2 above.

4. Numerical results and discussions

4.1. Laminar premixed flames

The performance and predictive capabilities of the FPI approaches are first investigated for stationary one-dimensional laminar premixed methane–air flames with equivalence ratios ranging from $\phi = 0.4$ to $\phi = 2.0$. A two-dimensional rectangular grid with dimensions 50 mm by 0.65 mm was used for this case. A highly stretched mesh of size 2 cells by 160 cells was used. The finest grid size near the flame front was of the order of 0.01 mm and the coarse grid size near the boundary was of the order of 1.2 mm.

The Cantera package was used to obtain solutions for one-dimensional laminar premixed flames needed for generating the FPI look-up table. Sixty-four solutions corresponding to different equivalence ratios in the flammability limit ranging from $\phi = 0.4$ to $\phi = 2.0$ were used. For each value of ϕ , the premixed flame solution contained 155 points in c -space. These points were non-uniformly distributed such that there were more points in regions of high gradients.

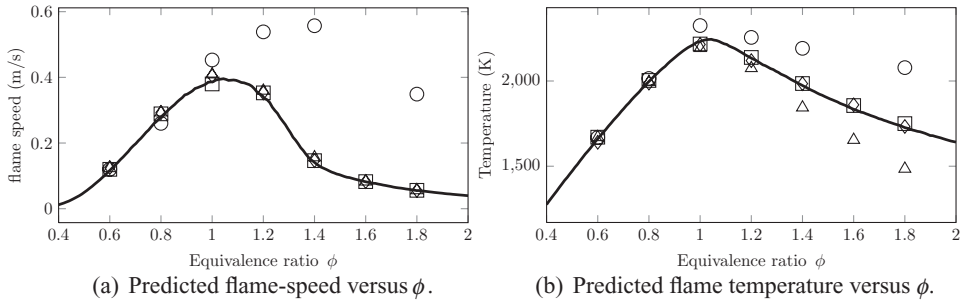


Figure 3. Predicted solutions of one-dimensional laminar methane-air premixed flames. Line: Detailed chemistry, square: FPI-Approach 1, triangle: FPI-Approach 2, diamond: FPI-Approach 3, circle: one-step mechanism.

Figures 3(a) and 3(b) compare the results obtained using the three FPI approaches to directly-calculated results obtained using both the one-step mechanism and the full GRI-Mech 3.0 mechanism without any tabulation. Both the predicted flame speed and burnt-gas or flame temperature are shown. Figure 3(a) shows extremely good agreement between the laminar flame speeds predicted by all three FPI approaches and the detailed chemistry solution using Cantera over the entire flammability range. Not surprisingly, there is also a significant improvement over the results obtained from the simplified one-step mechanism, which without modification cannot accurately predict the flame speed for the entire flammability range. It should be noted that all of the FPI predictions were made using the reduced set of ten species, as discussed earlier in Section 2.2. These results show that the reduction procedure is a valid simplification for controlling the size of the look-up table, as was shown previously by other authors [23,32]. However, the comparisons of flame temperature in Figure 3(b) clearly show the differences between the reaction rate tabulation method and mass fraction tabulation methods. FPI-Approach 2 under-predicts the burnt gas temperature for rich flame conditions. Figure 4 takes a closer look at the species mass fractions predicted by each FPI-Approach. The results of the figure show that the mass fractions of some minor species, like OH and CO, are poorly predicted by FPI-Approach 2. This occurs because the magnitudes of the reaction rate gradients for these species are very large near the flame front and the discretization of c -space using 155 points is not sufficient to accurately capture the solution of minor species. A significantly higher number of tabulated points in c -space would be required to remedy this situation. It is for this reason that only FPI-Approaches 1 and 3 have been used in the remainder of the laminar flame validation cases to follow.

As FPI-Approach 3 is based on the reconstruction of reaction rates, it is also of interest to show how well the method predicts the reaction rate values for different species for the laminar premixed case. Figure 5 compares the reaction rate predicted by Cantera and the reconstructed reaction rate predicted by FPI-Approach 3. The predictions are almost exact, both in their shape and magnitude.

4.2. Laminar counter-flow methane-air flame

The SLFM approach is based on the assumption that for the same value of a conserved scalar at any point in the flow, the local structure of a general laminar diffusion flame is the same as that of any simplified laminar diffusion flame. Most commonly, the detailed

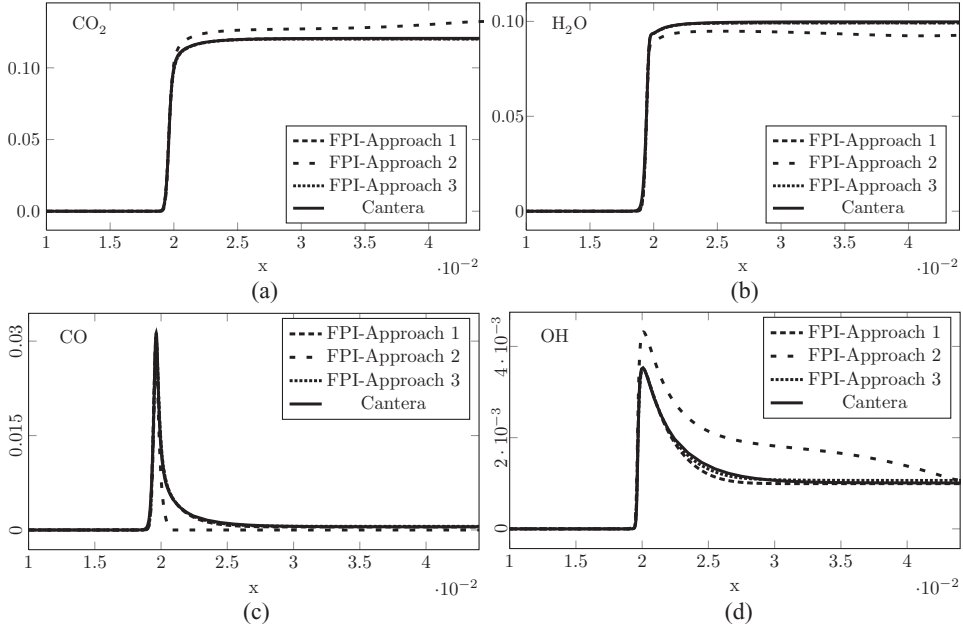


Figure 4. Predicted variation of species concentrations through flame obtained using the three different FPI coupling schemes for $\phi = 0.8$.

chemistry solutions of simplified one-dimensional counter-flow diffusion flames are used to generate flamelet libraries which can be used for more complex flow geometries, as proposed by Peters [11]. It is therefore important to compare the performance of the FPI approach with SLFM for predicting the counter-flow diffusion flames, as FPI uses the premixed flamelet solutions for predicting diffusion flames.

The experimental set-up by Puri and Seshadri [45] for an opposed-jet flame was used as the first validation case for these purposes as it provides a good set of experimental data to which the numerical predictions can be compared. A methane–air counter-flow flame was set up using two ducts, each with an inner diameter of 2.54 cm and with a separation distance of 1.4876 cm. The axial velocities of methane and air were 76.8 cm/s and 73.4 cm/s,

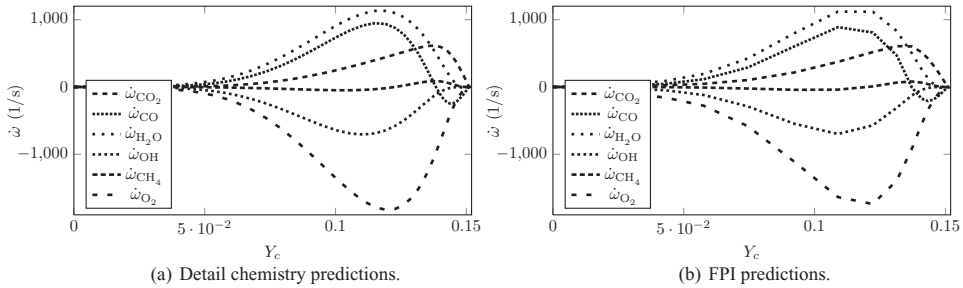


Figure 5. Predicted variations of the reaction rates for different species within a one-dimensional laminar methane–air premixed flame.

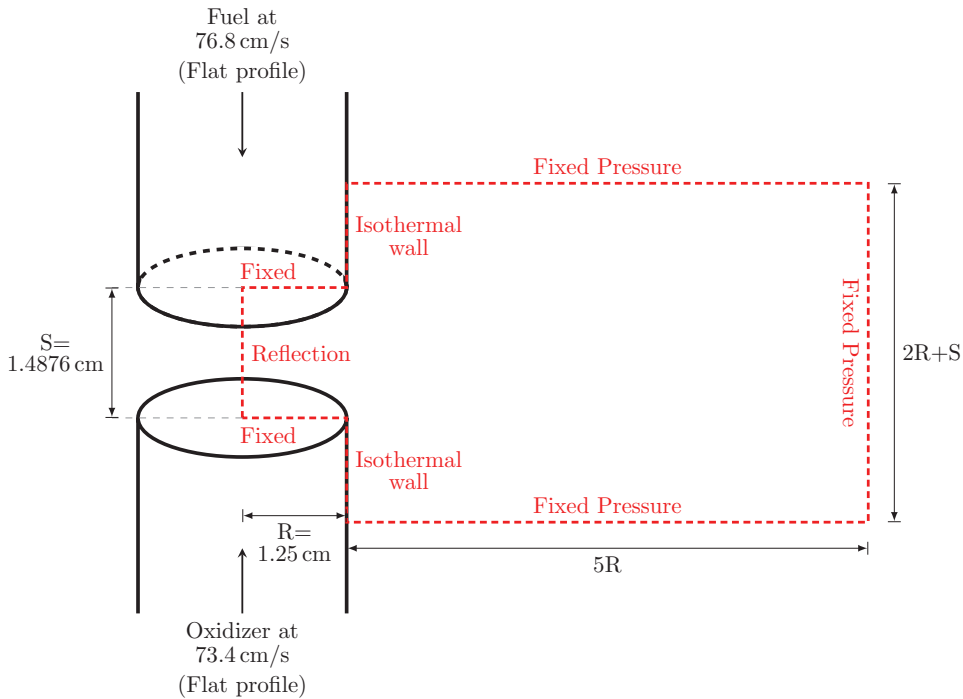


Figure 6. Schematic diagram showing the geometry and dimensions of counter-flow burner considered herein [45]. The red line shows the computational domain used to simulate the experimental set-up and the boundary conditions used. The symmetry of the burner geometry has been exploited to reduce the complexity of the problem from three space dimensions to two dimensions with an axis of symmetry.

respectively. A number of fine wire screens were placed in the duct to reduce turbulence ensuring a flat laminar velocity profile at the exit of the duct.

The initial grid and boundary conditions used for this problem is shown in Figure 6. A reflection boundary condition is used on the left boundary representing the symmetry plane. The inflow boundary conditions for both the ducts are kept fixed. All the far-field boundaries are set to constant atmospheric pressure and zero gradient for all other physical properties. The initial grid consists of 30 blocks, each block with 16 by 16 grid points.

After obtaining an initial approximate solution on the coarse grid, three levels of refinement were applied using the AMR capability of the solution method. The final grid for FPI-Approach 3 case after three levels of refinement is depicted in Figure 7(d). The refinement criterion was chosen to be the density gradient in order to track the region of maximum chemical activity. The new grid blocks are mostly concentrated halfway between the ducts along the flame. This example for the refined grid shows the potential of the AMR method, in terms of being able to refine areas of maximum activity. It should be noted that the predicted high temperature region in Figure 7 extends somewhat outside the mixing region. This can be attributed to the fact that, in the experimental set-up, an inert curtain of N_2 was used. The present numerical implementation was set up to handle only one fuel and one oxidizer stream, i.e., deal with a single mixture fraction variable. To account for another stream of flow, modifications to the present implementation would be needed to account for multiple streams and mixture fractions.

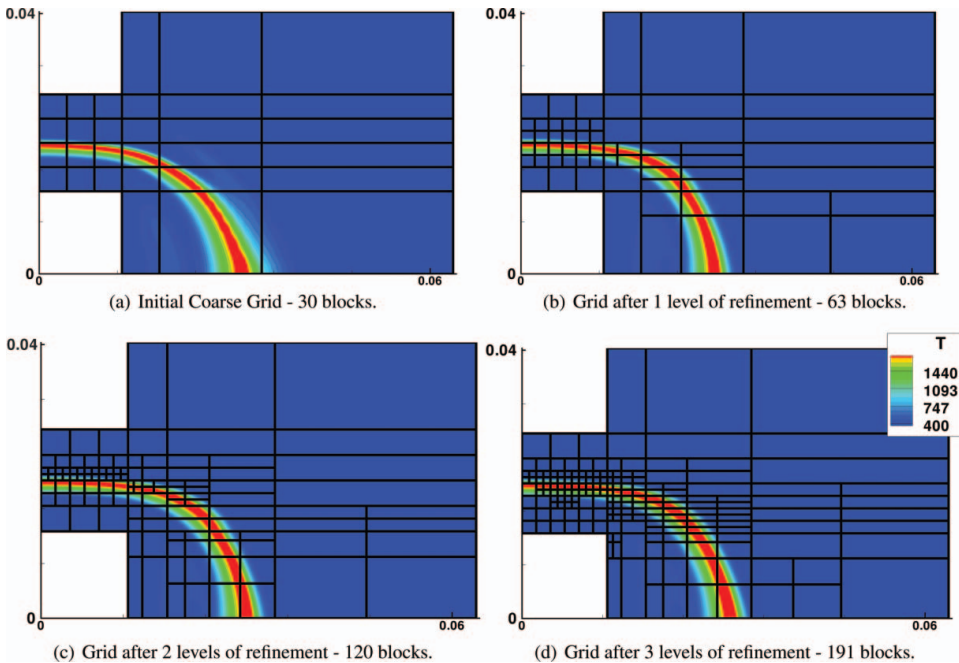


Figure 7. Predicted temperature distributions for laminar methane–air counter-flow flame illustrating the adaptive mesh refinement (AMR) scheme. Results are shown for the initial mesh as well as for the resulting computational mesh following three levels of AMR refinement. The computational grid is refined in regions of high temperature.

The centre-line profiles of temperature and major species predicted by both the SLFM and FPI methods are compared to the experimental data provided by Puri *et al.* [45] in Figures 8(a) and 8(b). It can be seen that all of the tabulation methods reproduce the species and temperature profiles reasonably well. The temperature profiles predicted by the tabulation methods however are shifted to the right as compared to the experimental results. The maximum temperature predicted by each numerical approach is summarized in Table 2. The flamelet approaches tend to over-predict the temperature, while the FPI approaches under-predict the temperature by almost the same magnitude. SLFM-Approach 2 has the best agreement with experiment, which is expected as it directly uses the temperature predicted by Cantera for the opposed jet diffusion flame. As a comparison, the one-step mechanism over-predicts the temperature by more than 200 K. It should be noted that an accurate prediction of temperature is required for NO_x prediction and inaccuracies in the temperature of 50 K are somewhat significant. Nevertheless, the progress of reaction variable would need to be redefined for FPI in order to predict NO formation [46–48].

Table 2. Maximum temperature predicted by different numerical methods for counter-flow methane–air flame.

Experimental	Cantera	One step	FPI Approach 1	FPI Approach 3	SLFM Approach 1	SLFM Approach 2
1950 K	1980 K	2169 K	1897 K	1912 K	2031 K	1985 K

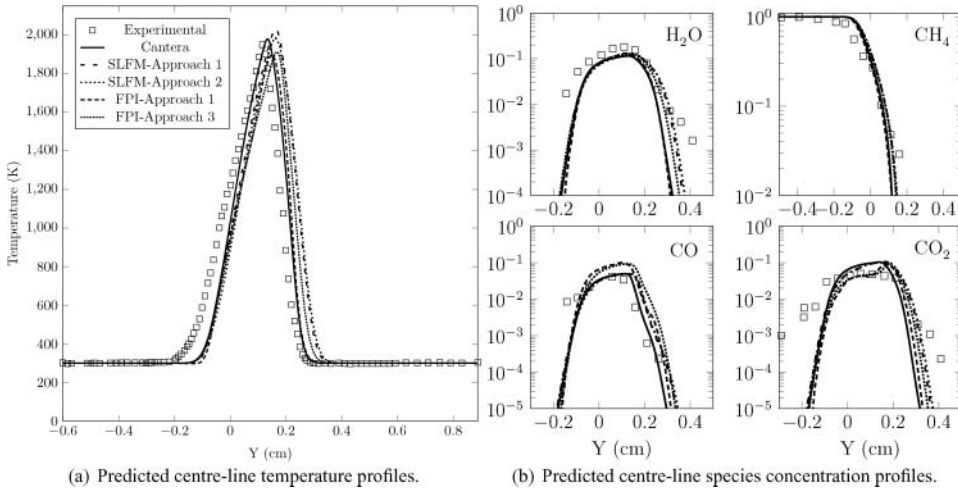


Figure 8. Comparison of predicted flow profiles and experimental results for the laminar methane–air counter-flow flame.

If one considers the prediction of carbon monoxide, the discrepancy in the maximum CO concentration relative to the experimental value is approximately a factor of two and are similar for both the FPI and SLFM approaches. This level of accuracy is similar to that obtained in the earlier numerical simulations of this counter-flow flame [45].

Figure 9 depicts predicted centre-line profiles of the mixture fraction, f , and the progress of reaction variable, Y_c , for the directly calculated computation obtained using Cantera and the various FPI and SLFM tabulated chemistry methods. The FPI and SLFM approaches appear to be able to reproduce quite accurately the profiles for the mixture fraction for this counter-flow case, whereas slightly larger errors are observable in the FPI methods predictions of the progress variable. The differences in the predicted values of Y_c would seem to be the cause of the observed errors in the predicted temperature profiles.

The preceding results quite clearly demonstrate that the FPI approach can quite successfully predict a counter-flow flame profile with virtually the same accuracy as the SLFM, a method based entirely on tabulated counter-flow solutions. The results therefore also provide strong justification for the use of the FPI methods based on premixed flamelets in the numerical simulation of more general diffusion flames.

4.3. Co-flow laminar diffusion flame

The FPI and SLFM approaches were also compared and assessed when applied to the solution of the steady co-flow laminar diffusion flame studied previously by Mohammed *et al.* [49], Day and Bell [50] and Northrup and Groth *et al.* [36]. Numerical predictions of this axisymmetric flame and burner were obtained on a computational domain that was rectangular in shape with dimensions 10 cm by 2.5 cm, as shown in Figure 10. The axis of symmetry was aligned with the left boundary and the right far-field boundary was taken to be a free-slip boundary. The top or outlet of the flow domain was open to a stagnant reservoir. The bottom or inlet was divided into three distinct regions. The innermost region was the fuel inlet which injects a nitrogen diluted methane fuel mixture ($Y_{CH_4} = 0.5149$, $Y_{N_2} = 0.4851$) at 298 K with a parabolic velocity profile having a maximum velocity of

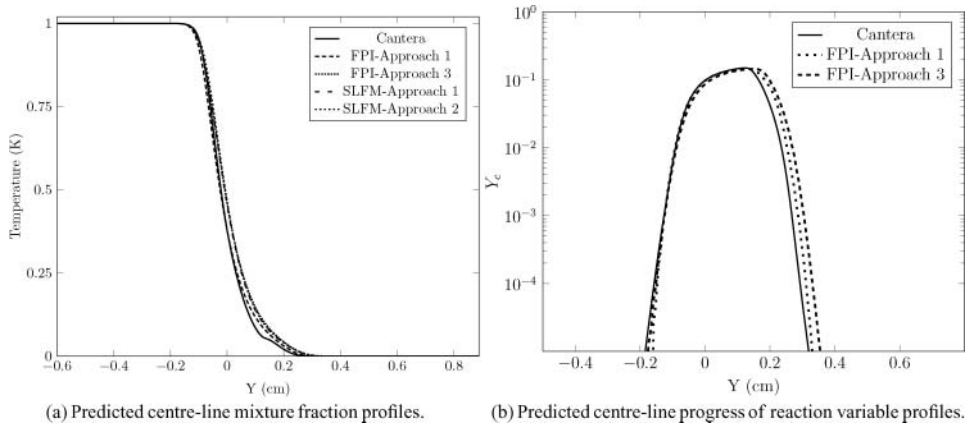


Figure 9. Comparison of predicted mixture fraction and progress of reaction profiles for different tabulation methods for the laminar methane-air counter-flow flame.

0.7 m/s. A second region representing the annular wall separating the fuel and oxidizer streams was followed by a third region containing co-flowing air at 298 K with a uniform velocity of 0.35 m/s.

As with the previous laminar flames, both the simple one-step and more detailed GRI-Mech 3.0 reaction mechanisms were considered for this co-flow diffusion flame. For the flame calculations, results were obtained for both mechanisms via direct calculation of the

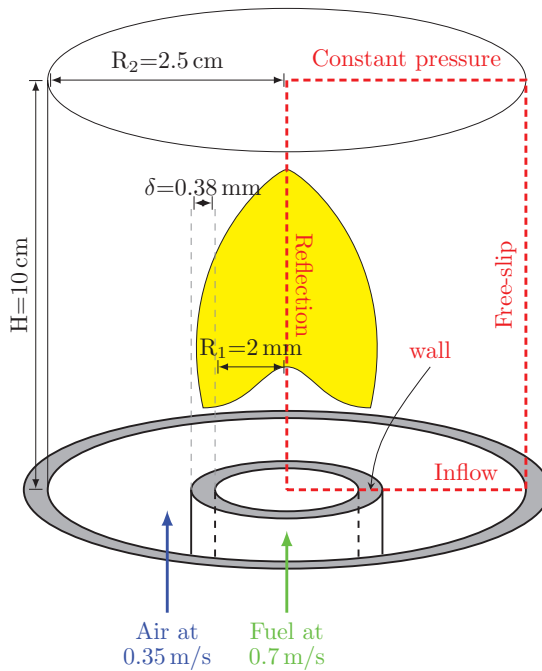
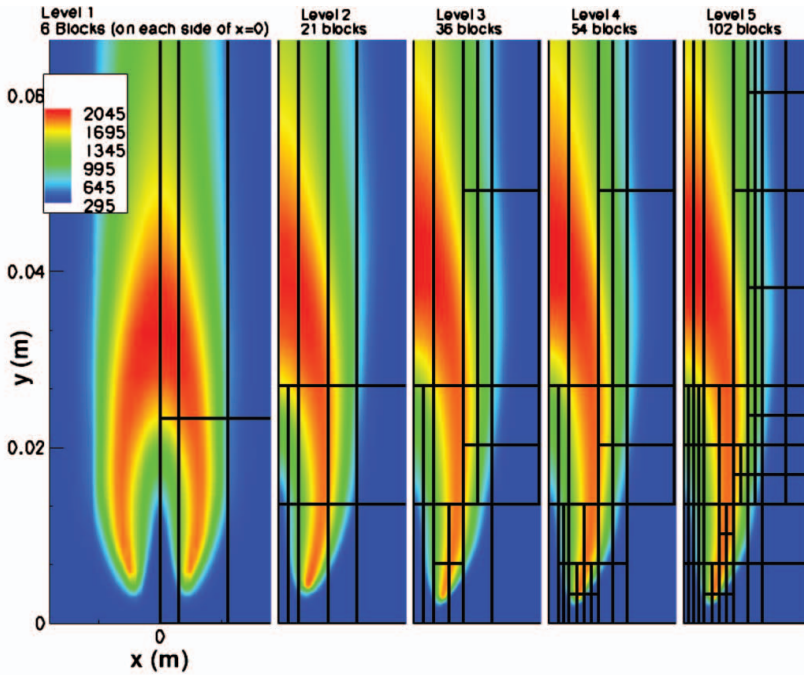
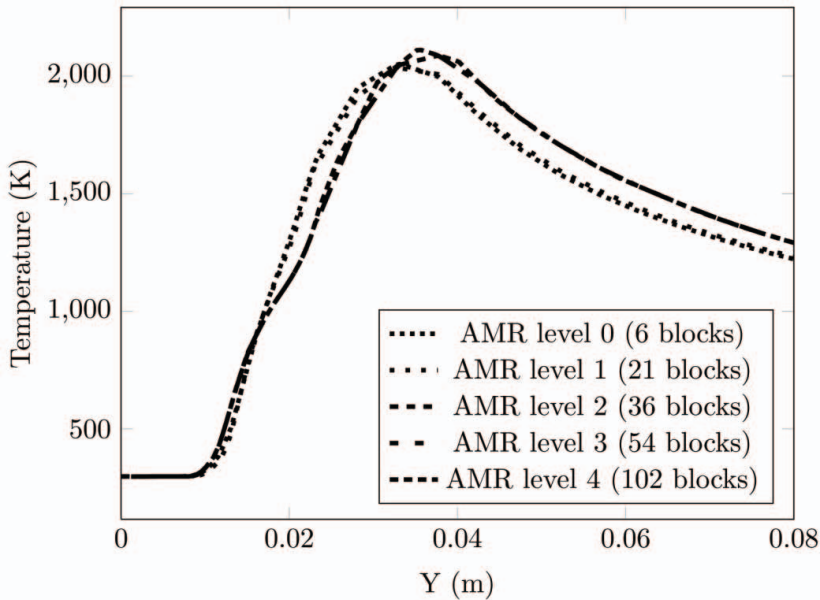


Figure 10. Schematic diagram of the flow geometry and computational domain used in predictions of co-flow laminar diffusion flame.



(a) Predicted temperature distributions on initial mesh and four refined grids obtained following four subsequent levels of mesh refinement for FPI-Approach 1 with GRI-Mech 3.0 mechanism.



(b) Predicted centre-line temperature profile after different levels of mesh refinement for FPI-Approach 1 with GRI-Mech 3.0 mechanism.

Figure 11. Predicted temperature distributions for co-flow laminar diffusion flame showing adaptive mesh refinement.

finite-rate chemical kinetics. The FPI tables were constructed using 100 values for Z and 155 values for Y_c for both mechanisms and solutions for FPI-Approaches 1 and 3 were determined. The SLFM approach was also used to obtain solutions for the detailed chemistry model. Solutions for SLFM-Approaches 1 and 2 were determined using a flamelet library storing solutions for 155 values of Z and 18 scalar dissipation rate values.

An initial computational mesh consisting of six 24×32 grid blocks and 4608 cells was considered first for the co-flow flame. Solutions were then obtained on successively refined meshes obtained by applying the AMR procedure. Solutions were obtained on grids consisting of 21 blocks and 16 128 cells, 36 blocks and 27 648 cells, 54 blocks and 41 472 cells, 102 blocks and 78 336 cells, respectively. The predicted temperature distributions obtained on the initial and four successively refined grids using FPI-Approach 1 are depicted in Figure 11(a). The figure illustrates well the capabilities of the AMR method to selectively refine the computational mesh in regions of high temperature variation and mixing. Figure 11(b) shows the centre-line temperature profile after different levels of refinement and it clearly shows that a grid converged solution is achieved after two levels of refinement. Based on the results of this mesh refinement study, a fixed computational mesh consisting of $24 \times 24 \times 32$ grid blocks and 18 432 cells was used for all of the comparisons of the results for different tabulation methods to ensure that the same mesh resolution was

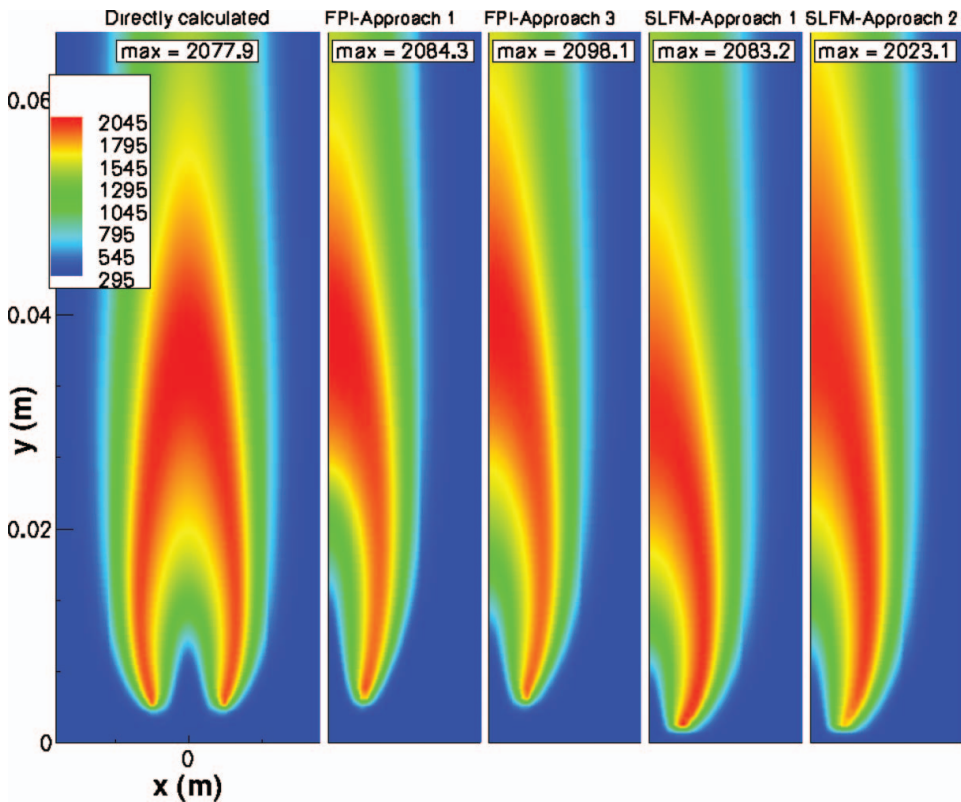


Figure 12. Comparison of predicted distributions of temperature for the methane-air laminar diffusion flame obtained using direct calculation and tabulated chemistry approaches with GRI-Mech 3.0 mechanism.

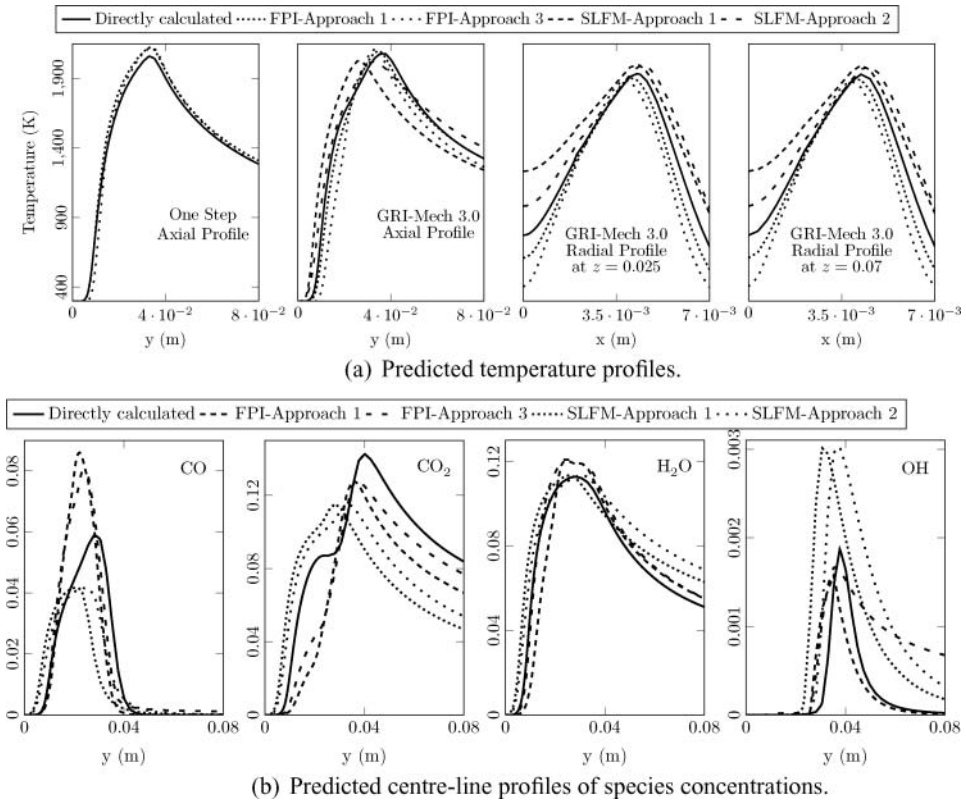


Figure 13. Comparison of predicted profiles for the methane–air co-flow laminar diffusion flame obtained using direct-calculation and tabulated chemistry on the 18 432-cell comparison mesh.

used in each case. For this comparison mesh, the smallest cell size was about 0.25 mm by 0.14 mm.

Predicted distributions of the temperature obtained using direct calculation and tabulated chemistry for FPI-Approaches 1 and 3 and SLFM-Approaches 1 and 2 with the GRI-Mech 3.0 mechanism are compared in Figure 12. All of the predictions shown in the figure were obtained using the 18 432-cell comparison mesh. Furthermore, predicted temperature profiles obtained using both the one-step and detailed chemical mechanisms on the 18 432-cell comparison mesh are shown in Figure 13(a). The two figures indicate that the FPI schemes predict the high-temperature regions of the flame much better than does the SLFM approach, for which this region is more spread out when the GRI-Mech 3.0 mechanism is used. The results also show that the predicted centre-line and radial temperature profiles of the directly-calculated solutions are quite accurately recovered by FPI approaches for detailed mechanisms. The SLFM-Approach 1 predicts the highest temperature much earlier than all other methods and the high temperature region in the SLFM-Approach 2 extends further downstream higher up in the flame than for the other approaches. Again not surprisingly, the maximum temperature predicted by the detailed-chemistry schemes are much closer to the experimental results reported by Mohammed *et al.* [49] than the results predicted by the simple one-step mechanism, indicating the importance of finite-rate

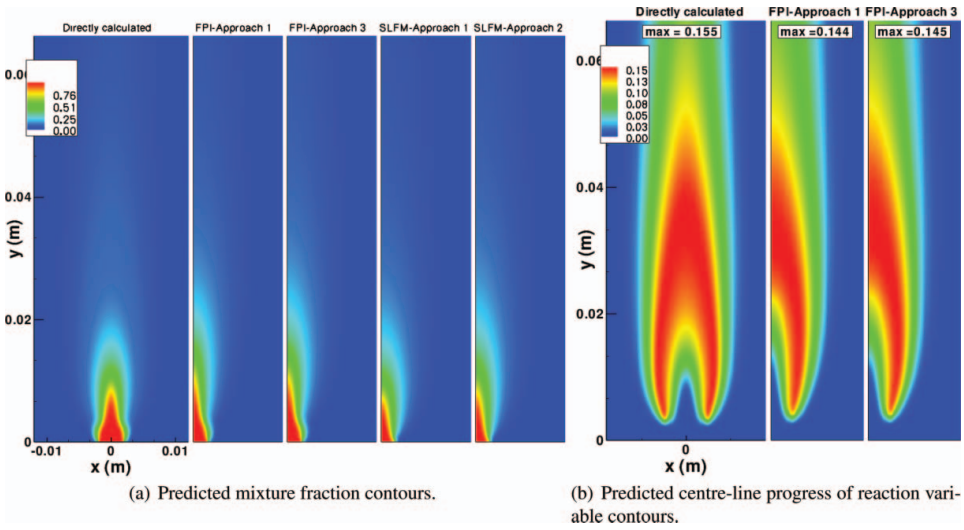


Figure 14. Comparison of predicted mixture fraction and progress of reaction contours for the laminar methane–air co-flow flame.

chemistry for diffusion flames of this type. An accurate balance between transport and chemical reaction rates is needed to predict accurately the flame temperature.

Predictions of the mass fraction of some major and minor species are shown in Figure 13(b). The FPI approaches reproduce the magnitude and profiles predicted by the detailed-chemistry very well. However, note that OH radical exhibits higher diffusion in the FPI-Approach 3 results. This can be probably attributed to the use of species transport equations only on the reduced set of tabulated species. However, the agreement between the maximum concentration of OH predicted by the FPI method and direct calculation is much better in comparison to that achieved by the SLFM.

Figures 14 and 15 depict predicted two-dimensional distributions and centre-line profiles of the mixture fraction, f , and the progress of reaction variable, Y_c , for the co-flow flame

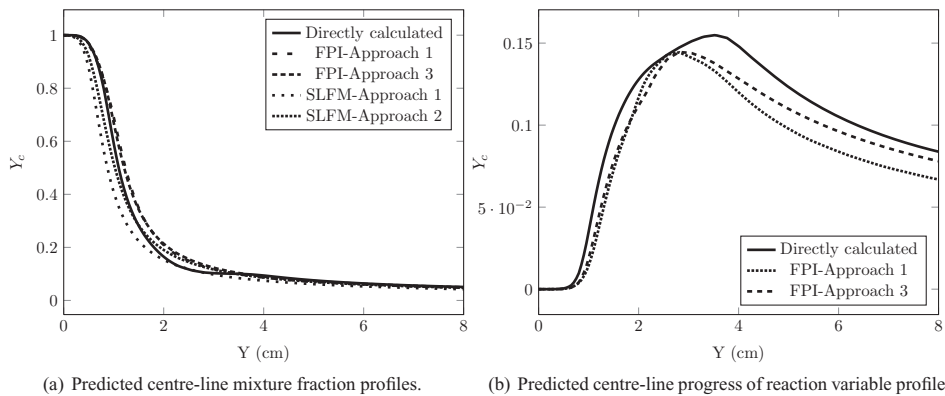


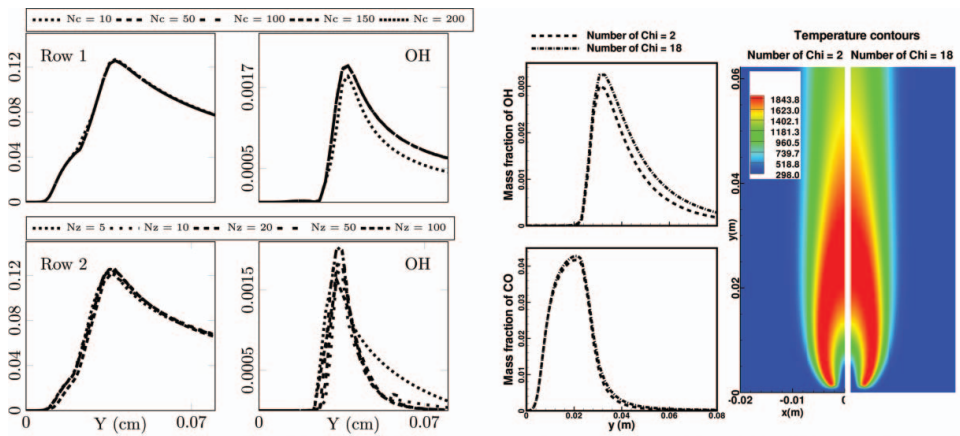
Figure 15. Comparison of predicted mixture fraction and progress of reaction profiles for the laminar methane–air co-flow flame.

Table 3. Comparisons of tabulated chemistry methods for methane–air diffusion flame with GRI-Mech 3.0 chemical mechanism.

	Directly calculated	FPI Approach 1	FPI Approach 3	SLFM Approach 1	SLFM Approach 2
Size of table	N/A	1.9 MB	1.9 MB	0.069 MB	0.0635 MB
CPU time/iteration·10 ⁻³	77.0 (10.84)	7.12 (1.03)	7.53 (1.09)	6.93 (1.0)	6.97 (1.001)
% time spent in reading tables	N/A	0.3	0.4	1.0	0.6
% time spent in calculating $\dot{\omega}_i$	43.04	N/A	0.4	N/A	N/A
Predicted flame height	3.56 cm	3.33 cm	3.52 cm	2.61 cm	3.26 cm
Predicted lift-off height	1.15 cm	1.25 cm	1.45 cm	0.08 cm	0.10 cm
Predicted max. temperature	2078 K	2084 K	2098 K	2083 K	2023 K

obtained using the directly calculated computation and the various FPI and SLFM tabulated chemistry methods. Again, the mixture fraction seems reasonably well predicted by all models, which is quite positive, but slightly larger errors are noticeable in the progress variable used in the FPI method. These errors in the progress variable would seem to correlate reasonably well with the observed errors in the predicted temperature field shown in Figure 12 above. These results, combined with those for the co-flow flame, strongly suggest that the errors in the predictions for the progress variable compared to directly calculated results is mostly affected by the treatment for the reaction rates (computed based on the premixed laminar flamelets) in the tabulated approach, and not by modelling of diffusion processes.

Table 3 provides a detailed summary of the comparisons between the tabulation methods and computational costs involved for the diffusion flame with the detailed GRI-Mech 3.0 mechanism. The advantages of the FPI over the flamelet approaches is again evident when



(a) FPI predictions of the profiles of the CO₂ and OH along the centre line of the methane-air laminar diffusion flame obtained with GRI-Mech 3.0 chemical mechanism using: (Top, Row 1) different numbers of c points in the FPI-Approach 3 table, (Bottom, Row 2) different number of z points in the FPI-Approach 1 table.

(b) SLFM predictions of the profiles of the mass fractions of OH and CO along the centre line and the distribution of the temperature for methane-air laminar diffusion flame obtained using two different flamelet libraries with GRI-Mech 3.0 chemical mechanism.

Figure 16. Effect of table size on numerical results of tabulated chemistry approaches.

Table 4. Maximum temperature calculated for the axisymmetric laminar diffusion flame using different numerical and chemical kinetic schemes. The maximum centre-line temperature reported by Mohammed *et al.* [49] is between 2025 K and 2029 K.

	Non-tabulated	FPI-Approach 1	FPI-Approach 3
GRI-Mech 3.0	2077.15 K	2084.31 K	2098.11 K
One-step	2181.20 K	2172.81 K	2168.99 K

considering some of the global properties of the flame predicted by each scheme. The FPI results are in much better agreement with directly-calculated results for overall flame height and lift-off height. Table 3 also shows that the CPU time per iteration is almost the same for the FPI and flamelet approaches. Moreover, all of these tabulation schemes are almost 11 times faster than directly solving the full set of species balance equations. This is because direct calculation of the reaction rates for the detailed methane–air chemical kinetic mechanism requires almost 43% of the computational time while evaluation and retrieval of tabulated data in the flamelet approaches requires less than 0.4% of the processor time.

In contrast to the results for the detailed mechanism, it is interesting that, for the one-step mechanism, use of the FPI tabulated approaches results in a slightly higher computational cost compared with the cost of the directly-calculated simulation. Tables 4 and 5 show the results and computational costs involved for one-step mechanisms. This is due to the additional overhead associated with interpolating tabulated values that is not offset by a significant reduction in the number of partial differential equations that must be solved. Obviously, the computationally payoffs of tabulation methods can really only be fully realized for larger reaction mechanisms.

Figure 16(a) provides an indication of how predicted species mass fractions are affected by the size of the FPI tables. The predicted centre-line profiles of the mass fractions of both major and minor species are depicted for differing numbers of Z and Y_c points in the FPI tables. It is evident that major species, such as CO_2 , are fairly independent of table size. However, for minor species, such as OH , the FPI predictions are more strongly dependent on the size of the table. For table sizes greater than 50 by 100, the results appear to be essentially independent of the tabulation procedure. Similarly, Figure 16(b) compares the results for two SLFM table sizes: one table built using only two values for the scalar dissipation rate, χ , and the other using 18 different values. Although major species are also not greatly affected by the size of the flamelet library, minor species exhibit slight variations from the directly-calculated results. It would seem for these near equilibrium flames, the SLFM results are not very sensitive to the number of tabulated scalar dissipation rates.

Table 5. CPU time required per iteration for the axisymmetric laminar diffusion flame using one-step mechanism.

	Non-tabulated	FPI-Approach 1	FPI-Approach 3
One-step	0.00396 (1)	0.00433 (1.09)	0.00436 (1.1)
GRI-Mech 3.0	0.0770 (19.44)	0.00712 (1.8)	0.00753 (1.9)

5. Conclusions

The SLFM and the FPI approaches have been compared extensively in the present study for laminar flames. The primary focus was to compare the performance of each approach for laminar diffusion flames. Two flames were studied: the methane–air opposed jet flame and a co-flow laminar diffusion flame. It was found that both FPI and SLFM can be successfully applied to the laminar diffusion flames and reproduce the effects of detailed chemistry and predict major and minor species concentrations at a much lower computational cost. The opposed-jet flame study results strongly demonstrate that FPI approaches, based on tabulated solutions of premixed flamelets, are capable of predicting diffusion flame structure as well, if not better, than flamelet approaches, which are based on tabulated solutions of steady diffusion flames. It was also found that SLFM approaches over-predict the concentrations of minor species in most regions of the co-flow flame. Similar findings have been reported in earlier studies of the SLFM approach. Also, the predicted flame height and lift-off-height of the FPI approaches are much closer to the directly-calculated chemistry results than those of the SLFM. The FPI approaches were found to be able to deal more readily with regions of high scalar dissipation rate of mixture fraction. Comparisons of predictions of mixture fraction and progress variable would suggest that the major source of error in the FPI method is associated with the use of the laminar flamelets in specifying the reaction rates, at least for the methane–air flames considered herein. These findings coupled with the ability of FPI approaches to handle both premixed and non-premixed flames, make the FPI tabulated approaches very appealing compared to SLFM approaches. While the concept of FPI tabulation is essentially an *ansatz* (i.e., an educated guess that is later verified by its results), the findings of the present study would certainly lend strong support for its use in the numerical prediction of combustion processes.

The effect of table size on the accuracy of predicted results was also examined. For FPI approaches, very coarse tables successfully reproduce the species concentrations of major species; however, more refined tables are needed to predict the minor species accurately. For the SLFM approach, it was found that for methane–air flames considered herein, the results are not greatly affected by the number of tabulated values used for the scalar dissipation rate.

Future research in this area will be directed to the application of the FPI tabulation method to turbulent flames using a presumed probability density function approach. Comparisons of a presumed conditional moment (PCM) FPI method to other subfilter-scale methods for the large-eddy simulation of turbulent premixed flames have already been carried out and reported in the recent studies by Perez *et al.* [51].

Acknowledgments

Financial support for the research described herein was provided by the MITACS (Mathematics of Information Technology and Complex Systems) Network, part of the Networks of Centres of Excellence (NCE) program funded by the Canadian government, as well as by Rolls-Royce Canada Inc. This funding is gratefully acknowledged with many thanks. Computational resources for performing the calculations reported herein were provided by the SciNet High Performance Computing Consortium at the University of Toronto and Compute/Calcul Canada through funding from the Canada Foundation for Innovation (CFI) and the Province of Ontario, Canada.

References

- [1] S. Delhaye, L.M.T. Somers, J.A. van Oijen, and L.P.H. de Goey, *Incorporating unsteady flow-effects in flamelet-generated manifolds*, Combust. Flame 155 (2008), pp. 133–144.

- [2] S.B. Pope, *Computationally efficient implementation of combustion chemistry using in situ adaptive tabulation*, *Combust. Theory Model.* 1 (1997), pp. 41–63.
- [3] N. Peters, *Reducing mechanisms*, 1991.
- [4] J.A. van Oijen and L.P.H. de Goey, *Modeling of premixed laminar flames using flamelet-generated manifolds*, *Combust. Sci. Technol.* 161 (2000), pp. 113–137.
- [5] S.H. Lam and D.A. Goussis, *Conventional asymptotics and computational singular perturbation for simplified kinetics modeling*, *Lecture Notes in Physics* 384 (1991), pp. 227–242.
- [6] U. Maas and S.B. Pope, *Simplifying chemical kinetics: Intrinsic low-dimensional manifolds in composition space*, *Combust. Flame* 88 (1992), pp. 239–264.
- [7] S.B. Pope and U. Maas, *Simplifying chemical kinetics: Trajectory generated low-dimensional manifolds*, *Mechanical and Aerospace Engineering Report: FDA 93-11* (1993).
- [8] M. Wang, J. Huang, A. Frisque, and W.K. Bushe, *Generating trajectories for low-dimensional manifolds using the stochastic particle model*, *Combust. Theory Model.* 12 (2008), pp. 249–267.
- [9] R.W. Bilger, *Turbulent flows with nonpremixed reactants*, *Turbulent Reacting Flows* 44 (1980), pp. 65–113.
- [10] P.A. Libby and F.A. Williams, *Turbulent flows involving chemical reactions*, *Ann. Rev. Fluid Mech.* 8 (1976), pp. 351–376.
- [11] N. Peters, *Laminar diffusion flamelet models in non-premixed turbulent combustion*, *Prog. Energy Combust. Sci.* 10 (1984), pp. 319–339.
- [12] M. Chen, M. Herrmann, and N. Peters, *Flamelet modeling of lifted turbulent methane/air and propane/air jet diffusion flames*, *Proc. Combust. Inst.* 28 (2000), pp. 167–174.
- [13] Z. Wen, S. Yun, M.J. Thomson, and M.F. Lightstone, *Modeling soot formation in turbulent kerosene/air jet diffusion flames*, *Combust. Flame* 135 (2003), pp. 323–340.
- [14] F. Liu, H. Guo, and G.J. Smallwood, *Evaluation of the laminar diffusion flamelet model in the calculation of an axisymmetric coflow laminar ethylene-air diffusion flame*, *Combust. Flame* 144 (2006), pp. 605–618.
- [15] M.D. Smooke, Y. Xu, R.M. Zurn, P. Lin, J.H. Frank, and M.B. Long, *Computational and experimental study of OH and CH radicals in axisymmetric laminar diffusion flames*, *Proc. Combust. Inst.* 24 (1992), pp. 813–821.
- [16] M. Nishioka, Y. Takemoto, H. Yamashita, and T. Takeno, *Effects of multi-dimensionality on a diffusion flame*, *Proc. Combust. Inst.* 26 (1996), pp. 1071–1077.
- [17] O. Gicquel, N. Darabiha, and D. Thévenin, *Laminar premixed hydrogen/air counterflow flame simulations using flame prolongation of ILDM with differential diffusion*, *Proc. Combust. Inst.* 28 (2000), pp. 1901–1908.
- [18] L. Vervisch, R. Hauguel, P. Domingo, and M. Rullaud, *Three facets of turbulent combustion modelling: DNS of premixed V-flame, LES of lifted nonpremixed flame and RANS of jet-flame*, *J. Turbulence* 4 (2004), pp. 1–36.
- [19] B. Fiorina, R. Baron, O. Gicquel, L. Vervisch, S. Carpentier, and N. Darabiha, *Modelling non-adiabatic partially premixed flames using flame-prolongation of ILDM*, *Combust. Theory Model.* 7 (2003), pp. 449–470.
- [20] B. Fiorina, O. Gicquel, L. Vervisch, S. Carpentier, and N. Darabiha, *Premixed turbulent combustion modeling using tabulated detailed chemistry and PDF*, *Proc. Combust. Inst.* 30 (2005), pp. 867–874.
- [21] J. Galpin, A. Naudin, L. Vervich, C. Angelberger, O. Colin, and P. Domingo, *Large-eddy simulation of a fuel-lean premixed turbulent swirl-burner*, *Combust. Flame* 155 (2008), pp. 247–266.
- [22] J.A. van Oijen, F.A. Lammers, and L.P.H. de Goey, *Modeling of complex premixed burner systems by using flame-generated manifold*, *Proc. Combust. Inst.* 127 (2001), pp. 2124–2134.
- [23] P. Domingo, L. Vervisch, and D. Veynante, *Large-eddy simulation of a lifted methane jet flame in a vitiated coflow*, *Combust. Flame* 152 (2008), pp. 415–432.
- [24] J.B. Michel, O. Colin, and D. Veynante, *Comparison of differing formulations of the PCM model by their application to the simulation of an auto-igniting H₂/air jet*, *Flow Turbulence Combust.* 83 (2009), pp. 33–60.
- [25] J.B. Michel, O. Colin, C. Angelberger, and D. Veynante, *Using the tabulated diffusion flamelet model ADF-PCM to simulate a lifted methane-air jet flame*, *Combust. Flame* 156 (2009), pp. 1318–1331.
- [26] N. Peters, *Turbulent Combustion*, Cambridge University Press, Cambridge, 2000.
- [27] D. Goodwin and H.K. Moffat, *Cantera*, <http://code.google.com/p/cantera/>.

- [28] H. Pitsch and N. Peters, *A consistent flamelet formulation for non-premixed combustion considering differential diffusion effects*, Combust. Flame 114 (1998), pp. 26–40.
- [29] S.K. Liew, K.N.C. Bray, and J.B. Moss, *A stretched laminar flamelet model of turbulent non-premixed combustion*, Combust. Flame 56 (1984), p. 199.
- [30] P. Domingo, L. Vervisch, and R.H. Sandra Payet, *DNS of a premixed turbulent V flame and LES of a ducted flame using a FSD-PDF subgrid scale closure with FPI-tabulated chemistry*, Combust. Flame (2005), pp. 566–586.
- [31] B. Fiorina, O. Gicquel, L. Vervisch, S. Carpentier, and N. Darabiha, *Approximating the chemical structure of partially premixed and diffusion counterflow flames using FPI flamelet tabulation*, Combust. Flame 140 (2005), pp. 147–160.
- [32] J. Galpin, *Modélisation LES de la combustion avec une prise en compte des effets de cinétique détaillée et en perspective d'application moteur*, PhD thesis, IFP, Division Techniques d'Applications Énergétiques, September 2007.
- [33] R. Vicquelin, B. Fiorina, S. Payet, N. Darabiha, and O. Gicquel, *Coupling tabulated chemistry with compressible CFD solvers*, Proc. Combust. Inst. 33 (2011), pp. 1481–1488.
- [34] K. Kuo, *Principles of Combustion*, John Wiley, New York, 1986.
- [35] R. Aris, *Vectors, Tensors and the Basic Equations of Fluid Mechanics*, Dover Publications, New Jersey, 1989.
- [36] S.A. Northrup and C.P.T. Groth, *Solution of laminar diffusion flames using a parallel adaptive mesh refinement algorithm*, Paper 2005–0547, AIAA, January 2005.
- [37] X. Gao and C.P.T. Groth, *A parallel adaptive mesh refinement algorithm for predicting turbulent non-premixed combustions flows*, Int. J. Comput. Fluid Dyn. 20 (2006), pp. 349–357.
- [38] M.R.J. Charest, C.P.T. Groth, and O.L. Gülder, *A computational framework for solving laminar reacting flows with soot formation*, Combust. Theory Model. 14 (2010), pp. 793–825.
- [39] X. Gao, S.A. Northrup, and C.P.T. Groth, *Parallel solution-adaptive method for two-dimensional non-premixed combustions flows*, Prog. Comput. Fluid Dyn. 11 (2010), pp. 76–95.
- [40] J.O. Hirschfelder, C.F. Curtiss, and R.B. Byrd, *Molecular Theory of Gases and Liquids*, John Wiley, New York, 1969.
- [41] C.R. Wilke, *A viscosity equation for gas mixtures*, J. Chem. Phys. 18 (1950), pp. 517–519.
- [42] C.R. Mathur, P.K. Tondon, and S.C. Saxena, *Thermal conductivity of binary, ternary and quaternary mixtures of rare gases*, Mol. Phys. 12 (1967), pp. 569–579.
- [43] C.K. Westbrook and F.L. Dryer, *Simplified reaction mechanisms for the oxidation of hydrocarbon fuels in flames*, Combust. Sci. Technol. 27 (1981), pp. 31–43.
- [44] G.P. Smith, D.M. Golden, M. Frenklach, N.W. Moriarty, B. Eiteneer, M. Goldenberg, C.T. Bowman, R.K. Hanson, S. Song, W.C. Gardiner, V.V. Lissianski, and Z. Qin, *GRI-Mech 3.0*, http://www.me.berkeley.edu/gri_mech/.
- [45] I.K. Puri, K. Seshadri, M.D. Smooke, and D.E. Keyes, *A comparison between numerical calculations and experimental measurements of the structure of a counterflow methane-air diffusion flame*, Combust. Sci. Technol. 56 (1987), pp. 1–22.
- [46] F. Biagioli and F. Güthe, *Effect of pressure and fuel-air unmixedness on NO_x emissions from industrial gas turbine burners*, Combust. Flame 151 (2007), pp. 274–288.
- [47] M. Wang, J. Huang, and W.K. Bushe, *Simulation of a turbulent non-premixed flame using conditional source-term estimation with trajectory generated low-dimensional manifold*, Proc. Combust. Inst. 31 (2007), pp. 1701–1709.
- [48] G. Godel, P. Domingo, and L. Vervisch, *Tabulation of NO_x chemistry in large-eddy simulation of non-premixed turbulent flames*, Proc. Combust. Inst. 32 (2009), pp. 1555–1561.
- [49] R.K. Mohammed, M.A. Tanoff, M.D. Smooke, A.M. Schaffer, and M.B. Long, *Computational and experimental study of a forced, time-varying, axisymmetric, laminar diffusion flame*, in *Twenty-Seventh Symposium (International) on Combustion*, Pittsburgh, 1998. The Combustion Institute, pp. 693–702.
- [50] J. Bell, M. Day, A. Almgren, M.J. Lijewski, and C.A. Rendleman, *Adaptive numerical simulation of turbulent premixed combustion*, in *Proceedings of the First MIT Conference on Computational Fluid and Solid Mechanics*, June 2001, p. 1.
- [51] F.E. Hernández-Pérez, F.T.C. Yuen, C.P.T. Groth, and O.L. Gülder, *LES of a laboratory-scale turbulent premixed bunsen flame using FSD, PCM-FPI and thickened flame models*, Proc. Combust. Inst. 33 (2011), pp. 1365–1371.